Glomerular Elasticity and Gene Expression Patterns Define Two Phases of Alport Nephropathy

Joonho Yoon*[1], Zhenan Liu*[1], Matthew Alaba[5], Leslie A. Bruggeman[6], Paul A. Janmey[7], Carlos A. Arana[2], Oluwatoyosi Ayenuyo[8], Isabela Medeiros[8], Sean Eddy[5], Matthias Kretzler[5], Joel M. Henderson[8], Abhijit Naik[5], Audrey N. Chang[1,4], R. Tyler Miller[1,3,4, #]

[1]Department of Internal Medicine, University of Texas Southwestern Medical Center, Dallas Texas, USA

[2]Department of Immunology, The University of Texas Southwestern Medical Center, Dallas, Texas, 75390, USA

[3]Medicine Service, VA North Texas Health Care System, Dallas, TX, USA.

[4]Pak Center for Mineral Metabolism and Clinical Research, UTSW Medical Center, Dallas Texas, USA

[5]Department of Internal Medicine, University of Michigan, Ann Arbor, Michigan, USA.

[6]Department of Inflammation & Immunity, Lerner Research Institute, Cleveland Clinic, Cleveland, Ohio, USA

[7]Department of Physiology and Institute for Medicine and Engineering, University of Pennsylvania, Philadelphia, PA, 19104, USA.

[8]Department of Pathology and Laboratory Medicine, Boston University Chobanian & Avedisian School of Medicine and Boston Medical Center, Boston, MA, USA

[#]Corresponding author- R. Tyler Miller, Nephrology, 8856, 5323 Harry Hines Blvd, Dallas TX 75390, 214-648-7214, tyler.miller@utsouthwestern.edu

The authors have declared that no conflict of interest exists.

*Co-first author. These authors contributed equally to this work.

Abstract.

Rationale- Mutations in *COL4A3,4, or 5* cause Alport syndrome and contribute to other glomerular diseases. Potential mechanisms include abnormal GBM structure, chemistry, elasticity, or ER stress. The causes of initial podocyte injury are not fully defined in collagen IV nephropathies.

Objectives- We characterized renal function, structural and biophysical properties of glomerular capillaries and podocytes, and renal gene expression patterns in *Col4a3*$^{-/-}$ mice (BL6) over the 8-month course of disease. To test for a role for ER stress, we treated Col4α3$^{-/-}$ mice with TUDCA.

Findings- *Col4a3*$^{-/-}$ mice develop proteinuria and reduced renal function at 4 – 5 months, but their glomerular capillaries become abnormally deformable, and podocytes are dislodged into the urine with volume loading at 3 months. Glomeruli become maximally deformable at 4 months with loss of 40% of their podocytes, and then stiffen progressively with progression of renal disease. In parallel, kidneys become increasingly fibrotic with proteinuria and inflammatory infiltrates as renal failure progresses. Bulk renal gene expression changes from 2 and 4 months where it shows increased expression of genes related to matrix organization, cytokine signaling, and cell injury to reduction in genes coding for differentiated renal tubular and metabolic proteins. Treatment of mice with TUDCA minimized glomerular injury, loss of renal function, and increased expression of genes that inhibit MAP, tyrosine kinase, and TGF-B.

Conclusion- Renal disease in *Col4a3*$^{-/-}$ mice progresses in two phases, before overt proteinuria with early podocyte injury and loss, and later with overt proteinuria and progressive fibrosis. Suppression of renal injury by TUDCA implicates ER stress and MAP, tyrosine kinase, and TGF-B signaling as a disease mechanism.

Introduction.

Many renal diseases including focal sclerosing glomerulonephritis (FSGS), IGA Nephropathy (IgAN), and Alport syndrome, caused by mutations in *COL4A3,4, or 5* begin with podocyte injury that is followed by varying degrees of proteinuria, hematuria, and tubulo-interstitial damage. The first evidence of podocyte injury is disruption of foot process architecture, foot process effacement, with their flattening, spreading, and loss of slit diaphragms. Further injury leads to detachment, loss of podocytes in the urine, and at some point, irreversible glomerular damage associated with tubulo-interstitial fibrosis and progression to end stage renal disease. The causes of early podocyte injury and related changes in gene expression are not fully defined. Additionally, *COL4A3,4,5* mutations are important beyond Alport syndrome because the heterozygous state is found increasingly in other more common glomerular diseases including FSGS and IgA Nephropathy(1). Thin Basement Membrane Nephropathy (TBMN), caused by heterozygous *COL4A3,4, or 5* mutations are increasingly recognized as a cause of chronic kidney disease(1-4).

Podocytes experience and accommodate traction and shear forces and contribute to a specific biophysical environment all of which depend on their unique cytoskeletal structure. That structure and cell function are maintained by factors that include attachment to the GBM, lateral attachment of foot processes to foot processes of neighboring podocytes, Ca fluxes, various signaling pathways, and mechanical environment (elasticity of the GBM, shear forces, and stretch)(5-12). In acute and chronic glomerular injury models including Alport syndrome, protamine, HIV nephropathy, ischemia and ischemia-reperfusion injury, the deformability of glomerular capillaries increases as a result of podocyte injury(10, 11, 13-15). Recent intravital imaging studies show distension of glomerular capillaries and aneurisms in glomeruli from *Col4a5*$^{-/-}$ mice at an early stage of disease, indicating increased deformability and reduced structural integrity of these capillaries(16, 17). Loss of podocytes reflects abnormal podocyte structure with reduced adhesion that may occur due to primary podocyte injury or abnormal matrix, and these two factors may be interrelated(7, 8, 10). Foot process effacement may represent a compensatory mechanism to maintain podocyte attachment to the glomerulus(18).

We used the C57BL/6J *Col4a3*$^{-/-}$ mouse model of Alport syndrome, a disease of glomerular origin, to study early steps in podocyte injury and responses with evolution of nephropathy. This model retains many essential

characteristics of the human disease, including accelerated podocyte loss, and has an 8 month time course allowing better time resolution of disease development and progression than other mouse strains(19-21). The abnormal GBM could injure podocytes through abnormal physical properties or abnormal signaling due to chemical differences in the normal compared to the Alport GBM(8, 22). Podocytes that normally produce COL4α3, 4, 5 could also be injured by accumulation of the mutant or misfolded collagen molecules with activation of the unfolded protein response (UPR, ER stress) and additional cell-specific remodeling pathways (23). Abnormal glomerular capillary mechanics caused by disordered cytoskeletal structure could also contribute to progressive podocyte injury though increased susceptibility to mechanical injury.

To distinguish among these injury mechanisms, we treated one group of *Col4a3*$^{-/-}$ mice with Tauroursodeoxycholic acid (TUDCA, *Col4a3*$^{-/-}$ -T), a compound that functions as a chemical chaperone and that protects cells from UPR-mediated injury or death(24-26). We analyzed renal function, glomerular capillary elasticity, structure, and bulk renal RNA expression over the course of disease. We find that Alport syndrome progresses in two phases, the first characterized by increasing capillary deformability and podocyte loss, and the second characterized by increasing proteinuria, decreasing renal excretory function, decreasing glomerular elasticity, and increasing expression of genes related to fibrosis and inflammation. TUDCA treatment suppressed the *Col4a3*$^{-/-}$ phenotype.

Results (2360 words).

Increased glomerular deformability precedes proteinuria and increased creatinine in Col4α3$^{-/-}$ mice. We studied the *Col4a3* mutant in the C57/Bl6 background to characterize the course of Alport nephropathy and glomerular capillary elasticity, a biophysical parameter that is poorly understood. An advantage of this mouse is its relatively long disease course with the opportunity for accurate timing of events. Although referred to as a knockout mouse for *Col4a3*, in fact the mutation is a truncation deleting the NC1 domain so that mRNA and protein presumably representing the 7S and collagenous domains are expressed (**Figure S1**)(19-21). In clinical settings, the development of proteinuria and/or increased serum creatinine mark the beginning of CKD, but these abnormalities lag glomerular and podocyte injury. We compared renal function and glomerular capillary elasticity, a marker of podocyte structural integrity, in *Col4a3*$^{-/-}$ mice and control littermates from 2 to 8 months of age. We measured increases in serum creatinine (**Figure 1A**) and urine Albumin/Creatinine Ratio (ACR) (**Figure 1B**) beginning at 2 months of age. From 4 months, creatinine increased but did not reach statistical significance until 6 months and reached a maximum value of 61 µM at 8 months. Similarly, urine ACR increased from 0.82 at 3 months (vs 0.14 in Control) and 3.51 at 4 months (Control 0.059) to 122 at 8 months. Over this time course, the serum creatine and urine ACR values in the control mice did not change significantly.

In past work using models of acute and chronic kidney diseases, we found that glomerular capillary elasticity reflects the state of podocyte cytoskeletal structure and that with podocyte injury, capillaries have increased deformability (10, 11, 15). We measured glomerular elasticity (Young's modulus, E) in the control and KO mice from 2 to 8 months of age using micro-indentation (**Figure 1C**)(27). The values of E for both the control and *Col4a3*$^{-/-}$ mice, were indistinguishable at 2 months (both 2.2 ± 0.2 kPa) and the values for the control mice remained essentially unchanged from 2 to 8 months. However, in the *Col4a3*$^{-/-}$ mice, the E values for glomeruli began to decrease at 3 months (1.85±0.09 kPa) and reached a minimum (1.56 ± 0.3 kPa) at 4 months of age. E then increased to values significantly greater than control by 7 months, reaching a maximum at 8 months (2.7 ± 0.1 kPa). These directionally opposite changes in elasticity early and late in disease signify distinctly different structural and functional properties of glomerular capillaries(10, 11, 28, 29). The early time point at which reduced glomerular E appears, before increases in serum creatine and with a minor increase in urine ACR,

indicates that podocyte injury begins early in the course of renal disease, and is sufficiently severe to affect overall glomerular capillary mechanical properties.

To assess gene expression patterns in the *Col4a3*$^{-/-}$ kidneys compared to Control over the course of renal disease, we performed bulk RNAseq of renal cortex at 2, 4, and 7 months, and identified 1346 differentially-expressed genes (DEGs) between WT and *Col4a3*$^{-/-}$ (KO) mice. **Figure 1D shows** a heatmap with expression of genes grouped vertically by function, and from 2 to 7 months horizontally with each column representing a separate mouse. The gene expression patterns change as a whole over time, but not dramatically at 2-4 months, reflecting the patterns in renal function and histology. However, at 7 months, reflecting disease progression from 4 to 7 months, in general, the changes are dramatic. Upregulated pathways include those involved in chronic inflammation and fibrosis, innate immunity, and cytokine signaling. Gene Ontology (GO) analysis shows that Inflammation is the principal response in KO kidneys, is detected as early as 2 months, and becomes prominent at 7 months. Upstream regulator analysis shows that these processes are driven by cytokines including Ifn-γ, TGF-β1, IL-1β, TNF, IL-6, and IGF1-activated pathways. The levels of renal injury marker expression, HAVCR1 (Kim1) and Lcn2 (NGAL) are increased at each time point compared to WT, but most dramatically at 7 months when the majority of the changes are statistically significant. EGF expression decreases minimally until 7 months when it decreased by half. Similarly, the expression of several kidney-specific transporters, Slc2a5 (Glut 5), Slc26a4 (Pendrin), Slc22a7 (OAT2), Aqp4, Slc16a4 (monocarboxylic acid transporter), and Slc12a3 (NCC) also decrease significantly only at 7 months. The expression of genes involved in inflammation and fibrosis (C3, TNF, Tlr8, Thrombospondin, Ltbp2, Inhibin, Col1a1, Col1a2, Col3a1, Lox (Lysyl oxidase) all increase. These results support the phenotypic data that show that renal injury is subtle up to 4 months but progresses dramatically and potentially irreversibly in the 4 – 7 month period. They further indicate that identifying disease mechanisms in the 0 – 4 month period may offer improved opportunities for intervention.

We then performed an independent component analysis (ICA), which is a statistical method that identifies clusters of highly correlated genes associated with specific functions. We identified a cluster, Cluster 6 (IC6), that was associated with proteinuria, comprising 253 genes. Using Enrichr-KG, we identified several interaction nodes through Gene Ontology (GO): Biological Function and the KEGG 2021 pathways, including Epithelial

Development, ECM-Receptor Interaction, Skin Development, Keratinocyte Differentiation, PI3K-Akt Signaling Pathway, Estrogen Signaling Pathway, Negative Regulation of Signaling, Staphylococcus aureus Infection, and IL-17 Signaling (**Figure S2**)(30). This pattern of gene expression and interactions suggests that in Col4α3-/- mice, processes such as renal epithelial cell growth, matrix remodeling, and cell adhesion are more active compared to WT mice and are associated with proteinuria. The involvement of IL-17 signaling is particularly notable given its role in innate immunity, responses to bacterial and fungal pathogens, the development of tissue-resident immune cells, its important role in the maintenance of epithelial barrier function, and tissue repair(31, 32).

To identify early gene expression changes related to progressive renal disease, we used a two-stage analysis method. First, we identified differentially-expressed genes at 7 months using hypothesis-driven selections based on functional characteristics, direction, and magnitude of change. We then focused our analysis of these genes at the two-month time point to investigate early gene changes (Supplemental Table X). This group of genes (Tnc, Col4a3, Lox, Scube1, MMP2 and TIMP1) were enriched for Biological Process modules Extracellular Matrix organization (GO:0030198) and a sub-set of those genes (Scube1, MMP2, and Timp1) identified the extracellular matrix disassembly module (GO:0022617). This subset also identified the cellular component disassembly module (GO:0022411). In the Reactome analysis, a group of eight genes (Col4α3, Lox, Scube1, MMP2, Timp1, Lcn2, Vim, and Cxcl1) appear in a network of interactions among Extracellular Matrix Organization (R-HAS-1474244), Signaling by Interleukins (R-HAS-449147), and Interleukin-4 and Interleukin 13 signaling (R-HAS-6785807) (**Supplemental Figure S3**). IL-4 and IL-13 have similar functions, are involved in wound healing, are produced by B cells, and signal through the JAK-Stat6 pathway(33, 34). Antibody-independent, and antigen-specific B cell production of IL-4 production in mouse glomeruli is sufficient to produce foot process effacement in mice, and IL-4 signaling is evident in glomeruli of some patients with minimal change disease(34, 35). These results indicate that processes that begin at 2 months in Col4α3$^{-/-}$ mice involving IL-4 and IL-13 signaling are early evidence of an immune component renal disease in this Alport model.

Using the IC6 gene list associated with proteinuria and GO and KEGG pathway and interactome analysis at 2, 4, and 7 months, we identified several interaction nodes, Epithelium Development, ECM-receptor interaction,

Skin development, Epithelium development, Keratinocyte differentiation, PI3K-Akt signaling pathway, Estrogen signaling pathway, Negative regulation of signaling, Staphylococcus aureus infection, and IL-17 signaling (**Figure S2**). This pattern of gene expression and interactions indicates that in the Col4α3$^{-/-}$ mice, renal epithelial cell growth, matrix remodeling, and cell adhesion are activated compared to the WT mice. The involvement of IL-17 signaling is interesting given its involvement in innate immunity, response to bacterial and fungal pathogens, development of tissue-resident immune cells, important role in maintenance of epithelial barrier function, and tissue repair(31, 32).

Evidence for unfolded protein pathway activation in Col4α3$^{-/-}$ podocytes. Podocytes, the cells that provide mechanical support for glomerular capillaries, determine the elastic properties of glomerular capillaries, and form the slit diaphragms, also produce and secrete the Col4α3,4,5 heterotrimer for the GBM(36). With loss-of-function mutations in any one of these proteins, podocytes must contend with a significant amount of inadequately processed collagen(23, 37, 38). Cells compensate for excess or misfolded protein by upregulating pathways that can improve folding and/or protein degradation including Bip (HSPA5), Xbp1s (Xbp1) and CHOP (DDIT3). We imaged WT and Col4α3$^{-/-}$ mouse cortex with confocal microscopy and found increased Bip expression in glomerular podocytes (**Figure 2A**). The levels of Bip, Xbp1s, and CHOP protein and mRNA are increased in the conditionally immortalized Col4α3$^{-/-}$ podocytes compared to their WT counterparts (**Figure 2B**). These cells were obtained from 3-month-old mice. WT cultured podocytes increase expression of Bip, Xbp1s, and CHOP in response to Tunicamycin, an agent that induces UPR, and the expression is reduced in a dose-response manner by treatment with TauroUrsoDeoxyCholic Acid, 3α,7β-Dihydroxy-5β-cholanoyltaurine (TUDCA), a chemical chaperone that is used in whole animals and cultured cells to suppress adverse effects of ER stress(24, 25, 39) (**Figure 2D**). For these reasons, we propose that an early step in podocyte injury could be UPR activation with disruption of normal protein processing and degradation, and that if the effects of UPR activation and podocyte remodeling could be suppressed, podocyte injury could be less severe or develop more slowly.

TUDCA treatment slows progression of renal disease in Col4α3$^{-/-}$ mice. Although ER stress activation due to Col IV misfolding was found in cultured cell-based systems, a mouse model, and human skin fibroblasts from Alport patients, protection from renal disease by inhibition of ER stress has not been demonstrated *in vivo*(23,

40). We tested the hypothesis that if collagen misfolding is the basis for podocyte injury in the Col4α3$^{-/-}$ mice, alleviation of ER stress would preserve renal function. Col4α3$^{-/-}$ mice were fed 0.8% TUDCA-incorporated into mouse chow from the time of weaning, 21- 25 days old, and 3 – 4 months before they developed proteinuria, until sacrifice(41). Normal littermates served as controls. We measured the effects of TUDCA treatment on Col4α3$^{-/-}$ mouse serum creatinine (**Figure 3A**), urine ACR (**Figure 3B**), and the Young's elastic modulus (E) of glomeruli (**Figure 3C**) at 4 and 7 months, the nadir and peak of glomerular E (**Figure 1C**). At 4 months, serum creatine and urine ACR values were similar among the Control, Col4α3$^{-/-}$, and TUDCA-treated Col4α3$^{-/-}$ (Col4α3$^{-/-}$-T) groups (**Figure 3**, left top two panels). However, at 7 months, when average serum creatinine and ACR were respectively 55±7 µm and 90±11, Col4α3$^{-/-}$-T values for creatine and ACR were respectively, 33±3.9 µm and 40±8.6, demonstrating reduced severity of glomerular capillary injury in the TUDCA-treated Col4α3$^{-/-}$ mice.

At 4 months, the value for E in the control mice was 2.1±0.04 kPa, 1.56±0.05 kPa for the Col4α3$^{-/-}$ mice, and 2.0±1.0 kPa in the Col4α3$^{-/-}$-T mice, indicating that podocyte injury-associated cytoskeletal changes are related to ER stress (**Figure 3C**). At 7 months, E for Control glomeruli was 2.1±0.06 kPa, and for the Col4α3$^{-/-}$ glomeruli it was 2.70±0.05 kPa, while the value for the Col4α3$^{-/-}$-T glomeruli was 1.9±0.04 kPa, a value comparable to control. These results demonstrate that TUDCA preserves the elastic properties of Col4α3$^{-/-}$ glomeruli, indicative of normalized podocyte cytoskeletal structure, and mitigates the rise in serum creatinine and urine ACR in these mice.

TUDCA treatment preserves Col4α3$^{-/-}$ kidney structure. Chronic kidney disease is marked by progressive fibrosis and loss of renal function, a component of which can be attributed to proteinuria(42). Our physiologic measurements at 7 months, late-stage disease, (**Figure 3A**) showed preserved renal function in the Col4α3$^{-/-}$-T mice implying preserved glomerular and renal structure. Low magnification kidney sections from 4-month mice stained with PAS or picrosirius red show that sections from control, Col4α3$^{-/-}$, and Col4α3$^{-/-}$+TUDCA mice are indistinguishable (**Figure S4, also see Figure 7**), indicating that at the 4 month time point, overall renal injury is minimal. At seven months (**Figure 3B**), the extent of injury in the Col4α3$^{-/-}$ kidneys are evident in the PAS and PSR-stained sections. Compared to the control kidneys, the PAS-stained Col4α3$^{-/-}$ kidneys show disrupted renal architecture, fibrosis, and inflammatory cell infiltrates. In the kidneys of Col4α3$^{-/-}$-T mice, these features are

present, but to a significantly lesser extent. The insets show representative images of glomeruli at each time point. The glomeruli from the Col4α3$^{-/-}$ mice are sclerotic and have excess, irregular PSR staining. Although glomeruli from the Col4α3$^{-/-}$-T mice are not normal, their structure is relatively preserved compared to the untreated Col4α3$^{-/-}$ glomeruli.

We measured the expression of genes associated with renal injury and fibrosis at 7 months using qRT-PCR of RNA samples from renal cortex in control, Col4α3$^{-/-}$, and Col4α3$^{-/-}$-T mice (**Table 1**). In Col4α3$^{-/-}$ mice, expression of Col1α1, Col1α2, Col3α1, lysyl oxidase (LOX), lysyl oxidase like 2 (Loxyl2), TGF-β1, CCN1 (Cyr61), a gene involved in development and wound healing and repair, and TNFα, all increased compared to Control. In the Col4α3$^{-/-}$-T mice, the mRNA expression for these genes was reduced significantly to levels intermediate between those in Control and untreated Col4α3$^{-/-}$ mice. EGF mRNA, a marker for renal parenchymal integrity, decreased significantly in the Col4α3$^{-/-}$ mice compared to Control, but in Col4α3$^{-/-}$-T mice, EGF mRNA was expressed at an intermediate level, significantly higher than Col4α3$^{-/-}$. These results demonstrate that TUDCA, initiated early in the course of disease, reduces glomerular injury and proteinuria, and slows progression of nephropathy in Col4α3$^{-/-}$ mice in part by reducing cytokine production and fibrosis.

To correlate the light microscopic findings showing reduced disruption of renal structure in response to TUDCA with molecular parameters, we compared bulk RNAseq at 4 months in WT, Col4α3$^{-/-}$, and Col4α3$^{-/-}$-T mice because this appeared to be the time point where course of renal disease changes with rising creatine, urine ACR, and maximum glomerular deformability changing to increasing rigidity. We compared three groups of 4 mice, WT, Col4α3$^{-/-}$, and Col4α3$^{-/-}$-T, and identified 1346 DEGs in the WT- Col4α3$^{-/-}$ comparison, and 129 DEGs between Col4α3$^{-/-}$ and Col4α3$^{-/-}$-T mice. The top 50 increased bottom decreased genes from each comparison are shown in supplemental tables 2-5. At 4 months, Col4α3$^{-/-}$ kidneys were enriched in genes related to extracellular matrix organization (GO:R-HAS-1474244), signaling by interleukins (R-HSA449147) mediators of inflammation, cell signaling, and cytoskeleton and adhesion (Supp Table 6. The expression levels of renal injury markers, HAVCR1 (Kim1) and Lcn2 (NGAL) increased in the Col4α3$^{-/-}$ mice, but had insignificant responses to TUDCA. Similarly, TUDCA did not have significant effects on genes associated with collagen or fibrosis, inflammation, or transporters (**Figure 4**). However, TUDCA increased the expression of genes that inhibit the

MAP kinase pathway (Dusp5, 6, 9) tyrosine kinase signaling Spred1, 2, Spry2) inhibit metalloproteases (TIMP3), and promote wound healing (FGF10) (Supplemental Table 7). Our inability to see an effect of TUDCA on expression of the injury marker, fibrosis, and cytokine genes at 4 months while the effects were clear at the tissue level and qRT-PCR for genes in this group at 7 months may relate to the fact that disease was relatively undeveloped at 4 months and the changes in the levels of expression of these genes were modest. Three genes related to UPR activation were differentially expressed in the Col4α3$^{-/-}$ - Col4α3$^{-/-}$-T comparison, Xbp1 (increased 1.85 X), Dnajb9 (increased 1.50 X), and Eef1akmt3 (decreased to 0.38 X)

Several other groups of genes showed interesting behavior with respect to TUDCA at 4 months. At this time point, the only genes related to UPR activation in the DEGs were Xbp1, Dnajb9, both of which increased in response to TUDCA, and Eef1akmt3, which decreased. Although tubular injury, for example in response to proteinuria can involve UPR activation, we suspect that at this point podocytes are the primary victims because they process mutant Col4α3,4,5 proteins, and the signal may be difficult to detect in bulk RNA. Expression of the podocyte-associated genes, Nphs1 (1.9 X), Nphs2 (2.1 X), Pdpn (2.25 X), Fat1(1.5 X) and Synpo (1.9 X) was increased in the Col4α3$^{-/-}$ mice compared to WT, while WT1, Cd2ap, and Actn4 were not differentially expressed. This pattern of gene expression changes suggests that Col4α3$^{-/-}$ podocytes are hypertrophic. The Vitamin D pathway also changed in response to TUDCA and disease. At 4 months, Cyp27b1 (1α(OH)Ase, rate limiting step for vitamin D synthesis) decreased 75% from untreated Col4α3$^{-/-}$ mice (no difference form WT), Cyp24a1 (Vitamin D 24-Hydroxylase, Vitamin D degradation) increased by 5.5-fold, and the vitamin D receptor (VDR) increased 1.75-fold. At 7 months, Cyp27b1 increases in Col4α3$^{-/-}$ mice compared to WT, while Cyp24a1 does not change.

TUDCA reduces podocyte loss from Col4α3$^{-/-}$ mouse glomeruli. Glomerular capillaries become deformable at 3 months, before an increase in creatine or urine ACR, suggesting that podocyte injury begins at or before that point. Alport patients lose podocytes in the urine at an accelerated rate, and can be detected before significant proteinuria develops(17). To identify the earliest time point for podocyte injury and determine whether podocytes loss relates to reduced glomerular E, we compared glomerular podocyte density in control, KO, and

TUDCA-treated Col4α3$^{-/-}$ mice at 2, 3, and 4 months using WT1 staining as a podocyte marker (**Figure 5**)(43). At 2 months, before measurable reduction in glomerular E, the podocyte density was similar among all three groups (Podocytes/10^6 μm^3 ± SD, Control 296±44, Col4α3$^{-/-}$ 276±39, and Col4α3$^{-/-}$+T 262±45). At 3 months, when increased glomerular deformability was detectable in the Col4α3$^{-/-}$ glomeruli, podocyte density remained unchanged in the three groups and comparable to the values for 2 month glomeruli (Podocytes/10^6 μm^3 ± SD, Control 285±35, Col4α3$^{-/-}$ 270±40, and Col4α3$^{-/-}$+T 299±32). In the 3 month Col4α3$^{-/-}$ mice, the SCr and ACR values were similar to those for the controls (SCr Col4α3$^{-/-}$ 12.9±0,81 vs 11.4±1.0 μM and ACR Col4α3$^{-/-}$ 0.82±0.13 vs 0.138±0.1 in Controls). However, at 4 months, we saw a clear reduction in podocytes in the KO glomeruli, and TUDCA treatment protected the Col4α3$^{-/-}$ glomeruli from podocyte loss (Podocytes/10^6 μm^3 ± SD, Control 276±48, Col4α3$^{-/-}$ 162±37, and Col4α3$^{-/-}$+T 246±40). At 4 months, when SCr (Col4α3$^{-/-}$ 14.8±-.67 vs Control 10.1±1.03) and urine ACR (Col4α3$^{-/-}$ 3.51±0.51 vs Control 0.059±0.02) were minimally elevated, but glomerular E in the Col4α3$^{-/-}$ mice was at its lowest point, the number of podocytes in the KO glomeruli was approximately sixty percent that of the control mice.

Early glomerular capillary deformability corresponds to reduced podocyte adhesion. Based on our measurements of decreased podocyte number in 4 month old Col4α3$^{-/-}$ mice and its correlation with changes in glomerular deformability, we assessed podocyte adhesion as a measure of early podocyte injury. Until 2 months of age, Col4α3$^{-/-}$ mice have normal renal function and glomerular elasticity, with increased capillary deformability first detectable at 3 months (**Figure 1C**). Based on our findings that approximately 40% of podocytes are lost in the Col4α3$^{-/-}$ mice at 4 months (**Figure 5**), we thought that podocyte injury should be detectable at 3 months, as decreased podocyte adhesion. To test this possibility, we measured podocyte adhesion in 3 month-old mice as urinary podocyte loss *in vivo* in response to volume loading. Mice were injected with 0.5N saline (80 μl/g IP), and urine was collected over two hours(44). Urinary podocytes that detached and were lost into the urine were quantified by two methods: by immunoblot of urine for nephrin, a podocyte-specific protein (**Figure 6A, B**), and counting WT-1 positive cells in the urine sediment (**Figure 6C**). With acute volume loading, the amount of urinary nephrin increased four-fold over control in the Col4α3$^{-/-}$ samples. TUDCA treatment reduced urine nephrin by approximately half. Loading for the nephrin immunoblots was normalized for creatinine. The number of podocytes that detached and were excreted in the urine of Col4α3$^{-/-}$ mice was increased compared to Control

(**Figure 5C**). These observations were consistent in 3 different experiments, where although the number of total podocytes lost in the urine varied from mouse to mouse, only the KO mice consistently had multiple WT-1 positive cells in their urine. In addition to the insignificant change in glomerular podocyte number in the Col4α3$^{-/-}$ and Control, mice the glomeruli had similar patterns of synaptopodin and nephrin staining consistent with similar numbers of podocytes in glomeruli and preserved structure in the 3 month KO mice (**Supp. Figure S6**). These results show that reduced podocyte adhesion and loss begin early in the course of nephropathy and suggest that early disease-associated structural alterations in podocytes including adhesion may contribute to the increased deformability of glomerular capillaries. TUDCA protects against podocyte loss at early stages of nephropathy.

TUDCA protects glomerular capillary and podocyte structure. Light microscopic images of glomeruli from 4 month old KO mice show generally preserved structure, but the glomeruli are hypertrophic compared to the control mice and have multiple dilated capillaries (**Figure 7, top row**). Additionally, focal lesions are present, but there is little evidence of tubulo-interstitial damage. The TUDCA-treated Col4α3$^{-/-}$ glomeruli show evidence of focal lesions and capillary dilation, but considerably less than the Col4α3$^{-/-}$ glomeruli. At 7 months, the patterns described above persist but in the Col4α3$^{-/-}$ mice are more severe. Glomerular hypertrophy and dilated capillaries remain evident. More glomerulosclerosis and focal glomerular lesions are present as well as significant tubulointerstitial injury and inflammation. The TUDCA-treated Col4α3$^{-/-}$ kidneys show less glomerular and tubulointerstitial injury compared to the Col4α3$^{-/-}$ kidneys, but injury has progressed from the 4 month time point (**Supplemental Table 1**).

We used transmission electron microscopy (TEM) to compare podocyte and GBM structures in our three groups of mice at 4 and 7 months (**Figure 8**). At 4 months, the glomeruli from the Col4α3$^{-/-}$ mice show regions of irregular GBM structure with thin and thick regions. The podocyte foot processes are normal in some regions but also show evidence of effacement and widened foot processes in other regions. Some podocyte cell bodies appear hypertrophic, exhibiting vacuolization, and have expanded ER indicative of ER stress (**Supplemental Figure S7, Table 12**. In the TUDCA-treated Col4α3$^{-/-}$ glomeruli, these pathologic findings are present, but less severe than in the Col4α3$^{-/-}$ mice. By 7 months, the pathologic changes in the Col4α3$^{-/-}$ GBMs and podocytes are more

advanced with evidence of substantial glomerulosclerosis. The pathologic findings are quantified in Supplemental Table 2.

Discussion.

We followed the course of nephropathy in Col4α3$^{-/-}$ mice (C57Bl6 strain) from 2 to 8 months of age to identify the mechanisms of podocyte injury at the earliest time points. We assessed renal function and structure as well as glomerular capillary and podocyte structure, function, and elastic properties. To identify early molecular processes that might be amenable to intervention, we measured whole kidney gene expression with RNAseq at 2, 4, and 7 months, and studied glomerular and podocyte characteristics at early time points, 3 and 4 months, before the mice developed significant proteinuria, reduced renal function, or parenchymal injury. Suspecting that processing of mutant Col4α3,4,5 heterotrimers could cause ER stress leading to podocyte injury and remodeling, we tested for a role for UPR activation by treating a group of Col4α3$^{-/-}$ mice with TUDCA, measuring ER stress-related gene expression at 4 months, and performing ultrastructural analysis.

We have three principal findings. First, in Col4α3$^{-/-}$ mice, Alport nephropathy has two distinct phases. In the first phase, birth through 4 months, podocyte injury and loss occur in the absence of significant proteinuria, reduced renal function, or parenchymal renal injury. Evidence of podocyte injury includes increased deformability of glomerular capillaries, reduced adhesion of podocytes to glomerular capillaries, and podocyte loss. During this period, renal genes associated with inflammation and fibrosis are activated, but not to levels sufficient to alter renal histology or function. The second phase, from 4 to 7 months, following loss of approximately 40% of podocytes, is characterized by progressive proteinuria, decreasing excretory function, progressive glomerulosclerosis, and tubulo-interstitial fibrosis. The second finding is that TUDCA, an agent that reduces the consequences of UPR activation, significantly slowed progression of renal disease in Col4α3$^{-/-}$ mice. This result, with increased expression of genes involved in the ER stress response and podocyte ER expansion in the Col4α3$^{-/-}$ mice indicates that UPR activation is a component of renal injury in this model. Our suppression of the Alport renal disease phenotype with TUDCA is the first demonstration that interfering with UPR activation suppresses the Alport renal disease phenotype and implicates the UPR pathway in the pathogenesis of the

disease. Third, podocyte injury occurs early in the course of nephropathy, before proteinuria or other phenotypic changes, and is characterized by increased capillary deformability, a potential therapeutic target, and reduced podocyte adhesion to capillaries.

Increased capillary deformability can be caused by podocyte injury, hypertrophy, or both, and probably represents a podocyte-specific remodeling program in response to injury(10, 11, 15, 45). Increased podocyte and capillary deformability may predispose to mechanical trauma and accelerate glomerular injury. This idea is consistent with the beneficial effect of ACEI/ARB therapy(46). The relevance of increased capillary deformability to the Col4α3$^{-/-}$ mouse model is evident from the studies of Gyarmati et al, who found dilated glomerular capillaries with aneurisms and thrombi in early-stage Col4α5$^{-/-}$ KO mice (C57/Bl6 background), similar to our results(16). The temporal association of podocyte loss with decreased glomerular E suggests a causal relationship. The first observed step in podocyte injury is rearrangement of podocyte cytoskeletal structures with effacement of foot processes, ultimately leading to loss, so a change in the biophysical properties of effaced or injured podocytes is a reasonable expectation.

Podocyte hypertrophy occurs in response to podocyte loss or hypertrophic stimuli where hypertrophy alone can cause podocyte injury(47). In our work, the minimum value for glomerular E, 1.6 kPa, occurs at 4 months when approximately 40% of the glomerular podocytes have been lost. At that time, we see foot process effacement, evidence of podocyte injury and hypertophy. As podocytes are lost from glomeruli, or in response to hypertrophic stimuli, they spread to cover denuded capillaries or maintain capillary coverage(48, 49). Hypertrophy is sufficient to increase the deformability of podocytes and glomerular capillaries. Cortes et al perfused glomeruli from control and remnant rat kidneys with hypertrophic glomeruli at progressively increasing pressures over the physiologic range and calculated values for compliance. Conversion of compliance to E results in a value 2.3 kPa in control glomeruli that is similar to ours, 2.2 kPa. In the remnant kidney glomerular E decreased by 40% to approximately 1.4 kPa, a value similar to our 4 month old Col4a3$^{-/-}$ mice(11, 45). These results indicate that either podocyte loss from glomeruli or glomerular hypertrophy, both situations where podocytes must change their structure to cover larger areas of GBM, are associated with reduced glomerular E, or increased deformability. In this setting, normal blood pressure is likely to injure podocytes and hypertension would be even more damaging.

The relationship between podocyte and GBM structure and the mechanical integrity of glomerular capillaries is not fully defined. In short-term studies where the structure of the GBM is unlikely to change, disruption of podocyte cytoskeletal structure and/or adhesion are sufficient to increase capillary deformability. Reinforcement of the actin cytoskeleton with agents such as Jasplakinolide, WNK1 kinase activation, or high Mg (increases Integrin affinity, F-actin) reduce capillary deformability. Similarly, chemical disruption of the podocyte cytoskeletons with actin depolymerizing agents, protamine, or WNK1 kinase inhibition increase deformability. These results demonstrate an essential role for podocytes in determining capillary wall mechanical properties(11, 29). Elastic environment and the mechanical behavior of neighboring cells can affect the mechanical properties of podocytes independently of the nature of the matrix(6, 10). In genetic experiments, the structure of the integrin-linked cytoskeleton can affect matrix composition by a mechanism involving recruitment of α-actinin-4 and PDLIM-5 to adhesomes by EPB41L5. Reduced recruitment of these proteins results in decreased adhesion strength and synthesis of matrix components, and increased recruitment has the opposite effect(8). Inflammatory injury of other glomerular cells may also contribute to podocyte injury(16). All of these factors probably contribute to aggregate tissue elastic properties and represent an integrated cellular response to injury.

We find reduced podocyte adhesion in 3 month Col4α3$^{-/-}$ mice, a time when we cannot detect podocyte loss and expect that glomeruli are normal at the light microscopic level. Podocyte injury probably begins perinatally with production of Col4α3,4, and 5. Podocytes would be exposed to protein that they cannot process and would activate pathways including the UPR to dispose of it. Additionally, they would be exposed to increased hemodynamic force from birth, a second insult possibly tolerated badly because of existing disordered protein processing and cytoskeletal remodeling in response. Using GO and pathway analysis covering 2 – 7 months, pathways related to epithelial cell development matrix structure, cell adhesion and inflammatory signaling including IL-17 are activated. At two months, GO analysis showed that extracellular matrix organization and disassembly pathways were activated as well as signaling by IL-4 and IL-13. At four months, the major active pathways in the WT – Col4α3$^{-/-}$ mouse comparison were extracellular matrix organization, inflammatory response, and cell-matrix adhesion, and involved increased expression of matrix, adhesion, cytokine, and chemokine genes.

At four months, the only physiologic evidence of renal injury in the Col4α3$^{-/-}$ mice was increased deformability of glomerular capillaries and podocyte loss, although transcriptomic analysis showed activation of fibrosis, cytokine, and chemokine pathways (**Figures 3, 5, 6**). The mice were treated with TUDCA beginning at weaning, or one month, and at four months, the only evidence of disease phenotype suppression by TUDCA was preservation of glomerular capillary elasticity and podocyte number, but without significant effects on renal transcriptomic injury markers, collagen or fibrosis genes, or inflammatory markers (**Figure 4B**). However, the effect of TUDCA on the renal disease phenotype in the Col4α3$^{-/-}$ mice and many of these genes at 7 months was dramatic (Table 1). Our inability to see clear effects of TUDCA on renal parenchymal injury at 4 months may related to the relatively low-level of inflammatory mediators and injury at this stage compared to seven months after development of high-grade proteinuria and the sensitivity of the bulk RNAseq method.

TUDCA is considered a chemical chaperone, and the effects of TUDCA on glomeruli and podocytes appear to involve reduction of ER stress. The effects of TUDCA are significant at four months (**Figures 3, 5, 6**) and probably involve suppression of UPR-mediated podocyte injury leading to improved elasticity, adhesion, and reduced proteinuria in these mice. TUDCA appears to have effects beyond those of a chemical chaperone that have been described as “anti-inflammatory”. Based on our results, it improves the viability of podocytes with misfolded collagen proteins as expected based on its chaperone role, but our differential expression data comparing Col4α3$^{-/-}$ and Col4α3$^{-/-}$-T podocytes suggest that TUDCA also increases expression of genes that suppress Ras-MAPK, tyrosine kinase, and FGF signaling as well as TGF-β-induced epithelial-mesenchymal transformation, and actin remodeling. These effects of TUDCA may contribute to its improvement in podocyte viability and suppression of tubule-interstitial in Alport nephropathy.

Methods.

Reagents. All fluorescent antibodies were purchased from Invitrogen. *Antibodies for immunofluorescence* **-** Col4α3: (Rat) Clone H31 97076), Chondrex, Inc.; Col4α3: (Rabbit) MBS2026491, BioSource; Bip: ab21685, Abcam; WT-1: sc-7385, Santa Cruz; Synaptopodin: sc-21537, Santa Cruz; Nephrin: AF3169, R&D Systems.

Antibodies for immunoblotting - Bip: ab21685, Abcam; Xbp1s: sc-7160, Cell signaling, and 24868-1-AP, Proteintech; Chop: (D46F1), #5554, Cell Signaling; GAPDH: XP, #5174S, Cell signaling; β-actin – #AM4302 Invitrogen.

Mouse breeding and treatment. Col4α3$^{-/-}$ mice in the C57Bl/6J background were obtained from Jeff Miner(20). Genotyping was performed by Transnetyx. For studies, homozygous males were bred with heterozygous females to obtain Col4α3$^{-/-}$ and Col4α3$^{+/+}$ mice. KO mice were fed 0.8% TauroUrsoDeoxyCholic Acid, 3α,7β-Dihydroxy-5β-cholanoyltaurine (TUDCA) incorporated into mouse chow from the time of weaning (25-28 days old) until sacrifice (24, 25, 39, 41). TUDCA (98% purity) was from Chemimpex and was incorporated into standard mouse chow by Teklad. Normal littermates served as controls.

We measured the serum creatinine either by submandibular puncture or exsanguination at the time of sacrifice. After clotting at room temperature for 1hr and centrifugation at 2000 x g for 10min, the supernatants were transferred to new clean tubes and stored at -80 °C for further analysis. Mouse urine samples were collected from spot urine in clean empty cages and centrifuged at 400 x g for 10min. The supernatant was transferred to new clean tube and stored at -80 °C. Urine albumin concentrations were measured using a Mouse Albumin ELISA Kit (Immunology Consultants Laboratory, Inc). Serum and urine creatinine levels were measured by UTSW O'Brien Kidney Research Center Physiology Core using capillary electrophoresis. Urine albumin-to-creatinine ratios were calculated to assess the severity of albuminuria.

Podocyte adhesion was measured in vivo by injecting 0.5N saline (80 µl/g IP), and collecting urine over two hours(44). An aliquot of urine was normalized for creatinine and immunoblotted for nephrin. Another aliquot was centrifuged, the sediment attached to a slide and stained for DAPI and WT-1.

Isolation of mouse glomeruli. To isolate glomeruli, kidneys were removed from mice, placed in iced buffer, decapsulated, and dissected on ice to isolate the cortices from the medullae. The cortices were minced with a razor blade and pushed through a screen (180 µm, W.S. Tyler Co, Cleveland, OH) with a flexible metal spatula. The minced tissue was suspended in PBS with 5.5 mM glucose and 0.3 mM pyruvate (GIBCO), filtered through a 90 µm nylon mesh (Falcon) to remove vessels and large pieces of tissue. The filtrate was collected in a 45 µm mesh nylon filter (Falcon) and contained intact glomeruli with minimal contamination (< 2%) by tubular cells(10,

11, 50). Glomeruli were maintained in DMEM with 0.1% FBS at room temperature before drug treatment, elasticity measurements or confocal imaging.

Podocyte cell line development and culture. Podocyte cell lines were derived from WT and Col4α3$^{-/-}$ primary podocyte outgrowths from glomeruli isolated from adult mice (12-16 weeks of age). Glomeruli were maintained in DMEM with 0.1% FBS at room temperature and seeded onto collagen I-coated dishes for 4-6 days to allow primary glomerular cell outgrowth. Primary podocytes were then trypsinized, filtered with 20 µm cell strainer, and re-plated for experiments or immortalization. Primary podocytes were conditionally immortalized by infection with a lentivirus expressing the temperature sensitive SV40 T antigen tsA58. Lentivirus was produced from pLenti-SV40-T-tsA58 (abm cat# LV629) as previously described (51) using the VSV envelope from pMD2.G (Addgene cat#12259, gift from Didier Trono) and the packaging plasmid pCMV delta R8.2 (Addgene cat # 12263, gift from Didier Trono). Primary glomerular outgrowths were infected for 48 hours followed by selection with puromycin (2ug/ml). Conditionally-immortalized mouse podocytes were cultured in RPMI 1640 with 10% FBS. Cells cultures were expanded at 33°C and for experiments, differentiated at 37°C for 7-10 days as previously described (52).

Animal Studies. Animal research was performed in accordance with the UT Southwestern Medical Center Animal IACUC guidelines. The research study protocol (number 2014-0078) was approved by the UT Southwestern Medical Center Animal IACUC (NIH OLAW Assurance Number A3472-01). UT Southwestern Medical Center is fully accredited by the American Association for the Assessment and Accreditation of Laboratory Care, International (AAALAC). Animals are housed and maintained in accordance with the applicable portions of the Animal Welfare Act and the Guide for the Care and Use of Laboratory Animals. Veterinary care is under the direction of a full-time veterinarian boarded by the American College of Laboratory Animal Medicine. Mice were sacrificed for experiments by first anesthetizing with Avertin and then euthanizing by exsanguination.

Kidney total RNA sample preparation for RNAseq. Kidneys from each group of mice were removed and 20 mg of cortex was processed for RNA purification. All samples were stored with RNA later in -80 °C and thawed for RNA purification. Total RNA was purified using Direct-Zol™ RNA Miniprep Plus (Zymo research) and the concentration was measured with DS-11 FX+ (Denovix). Final RNA samples were submitted for sequencing to

Next Generation Sequencing Core of UTSW. Sequence analysis and results were performed by the University of Michigan Nephrotic Syndrome Study Network (NEPTUNE).

Quantitative RT-PCR. Total RNAs were purified from each group of mouse cortex part using Direct-Zol™ RNA Miniprep Plus (Zymo research) and used for reverse transcription by SuperScript III First-Strand Synthesis System (Invitrogen). Quantitative PCR was carried out with specific primers using SYBR™ Green PCR Master Mix (Applied Biosystems) and StepOnePlus™ Real-Time PCR System (Applied Biosystems). For quantitative analysis, the samples were normalized to GAPDH (Glyceraldehyde 3-phosphate dehydrogenase) gene expression using the ΔΔCT value method. Primer sequences for specific genes are below. 5,27

Col1α1 forward: 5'-GGAGAGAGCATGACCGATGG-3' , reverse: 5'-AAGTTCCGGTGTGACTCGTG-3'

Col1α2 forward: 5'-GCTGGTGTAATGGGTCCTCC-3', reverse: 5'-ATCCGATGTTGCCAGCTTCA-3'

Col3α1 forward: 5'-AGGCTGAAGGAAACAGCAA-3', Col3α1 reverse: 5'-TAGTCTCATTGCTTGCGTG-3'

Col4a3 forward: 5'-CAAAGGCATCAGGGGAATAACT-3' (aa-88, N-terminal region, 7S domain), 5'-ATTAGTGGCAGAGCTCTCG-3' (NC-1 domain), reverse: 5'-ACCCTTAGATCCGTTGCATCC-3'

Col4a4 forward: 5'-TTTGGACAGGGTACAGCTTG, reverse: 5'-TAGTGGCACACTTGGTGGAT

Col4a5 forward: 5'-CTGGAAGAATGGGTCCAGAT, reverse: 5'-GTTCCTTTGAAACCTGGGAA

LOX forward: 5'-CCGGTTACTTCCAGTACGGT-3', reverse: 5'-ATCCGCCCTATATGCTGAAC-3'

LOXL2 forward: 5'-GGAAAGCCTACAAGCCAGAG-3', reverse: 5'-GCAGATACCAGGTCCCACTT-3'

TNFα forward: 5'-ACGTCGTAGCAAACCACCA-3', reverse: 5'-TTGTCCCTTGAAGAAAACCT-3'

TGFβ-1 forward: 5'-CAGTGGCTGAACCAAGGAG-3', reverse: 5'-ATCCCGTTGATTCCAGGTG-3'

EGF forward: 5'-ATCTGACTTCATGGAGACA-3', reverse: 5'-AACTGGCTCTGTCTGCCGT-3'

Cyr61 forward: 5'-GTGAAGTGCGTCCTTGTGGACA-3', reverse: 5'- CTTGACACTGGAGCATCCTGCA-3'

GAPDH forward: 5'-CCATGGAGAAGGCTGGGG-3', reverse: 5'-CAAAGTTGTCATGGATGACC-3'

Measurement of glomerular elasticity. The elastic moduli of glomeruli isolated from 3-6 month old mice were measured using a microprobe indenter device(10, 11, 27). Briefly, a tensiometer probe (Kibron, Inc, Helsinki) with a 250 μm radius flat-bottom needle was mounted on a 3-D micromanipulator with 160 nm step size (Eppendorf, Inc) attached to a Leica inverted microscope. A glass slide containing a dilute sample of glomeruli was imaged by bright field illumination and the bottom of the probe was brought through the air-water interface

until it was just above the surface of a single glomerulus of diameter approximately 60 μm. The probe was calibrated using the known surface tension of a pure water/air interface, and the stress applied to the probe as it was lowered onto the glomerulus was measured as a function of indentation depth. In principle, this deformation geometry is that of an infinite plane compressing a spherical object. The absolute values of elastic modulus can be calculated from appropriate models that require assumptions about the adherence of the glomerulus to the probe and the glass slide, whether the glomerular elasticity is modeled as a uniform sphere or an elastic shell, and other structural factors that confound calculation of the magnitude of elastic modulus from the force-indentation data alone. In all cases indentations were kept below 15 μm to avoid large strains that could damage the glomeruli. After the largest indentations, measurements were repeated at small strains to confirm that the deformations were recoverable.

Light microscopy of renal tissue. Formalin-fixed, paraffin-embedded kidney tissue was sectioned at 3 μm, and sections were stained with periodic acid-Schiff or picrosirius red stains. Stained tissue sections were examined, and digital images were collected under brightfield microscopy with an Olympus BX-80 microscope equipped with a Q-Imaging Retiga 2000R imaging system.

Immunofluorescence staining. Treated glomeruli were spun down at 5,000g for 5 min, resuspended and fixed in 4% paraformaldehyde for 30 minutes, and then washed 3x in PBS. Washed glomeruli were resuspended in PBS, 100 μl pipetted onto a slide, and attached to a coverslip overnight at 4˚C. The slide was rinsed in PBS to remove unattached glomeruli and further fixed with 4% paraformaldehyde for 1 hour at room temperature. Attached and fixed glomeruli on coverslips were then washed 3x in PBS, blocked with SEA BLOCK Blocking Buffer (PIERCE) for 40 minutes, then permeabilized with 0.5% Triton X-100 in PBS for 10 minutes. Glomeruli on coverslips were then stained using standard procedures, and imaging was performed using a Zeiss LSM 880 confocal microscope.

Confocal microscopy. Confocal imaging was performed in the Cell Biology and Imaging Core in the O'Brien Kidney Research Core, on a Zeiss LSM880 with Airyscan laser scanning microscope equipped with Plan-Apochromat 10x/0.3 NA, 20x/0.8 NA, 25x/0.8 NA and 63×/1.40 NA oil-immersion objective (ZEISS, Oberkochen, Germany). Fluorescence images were acquired using ZEN black 2.3 software with a 20x/0.8 NA or 63x/1.40 NA objective and Zeiss Immersion Oil 518F was used for the 63x/1.40 NA objective. Experiments were performed

at constant room temperature. Images or regions of interest (ROIs) were further processed with ZEN 2.6 (blue edition) software.

Electron microscopy. Tissue samples were fixed with 2.5% (v/v) glutaraldehyde in 0.1M sodium cacodylate buffer (pH7.4). After three rinses with 0.1 M sodium cacodylate buffer, samples were embedded in 3% agarose and sliced into small blocks (1mm^3), rinsed with the same buffer three times and post-fixed with 1% osmium tetroxide and 0.8 % potassium ferricyanide in 0.1 M sodium cacodylate buffer for one and a half hours at room temperature. Samples were rinsed with water and then block stained with 4% uranyl acetate in 50% ethanol for two hours. They were then dehydrated with increasing concentration of ethanol, transitioned into propylene oxide, infiltrated with Embed-812 resin, and polymerized in a 60°C oven overnight. Blocks were sectioned with a diamond knife (Diatome) on a Leica Ultracut 7 ultramicrotome (Leica Microsystems) and collected onto copper grids, post stained with 2% aqueous uranyl acetate and lead citrate. Images were acquired on a JEM-1400 Plus transmission electron microscope equipped with a LaB_6 source operated at 120 kV using an AMT-BioSprint 16M CCD camera.

Bulk RNA sequencing.

The total input of 100ng RNA was used for the library preparation on each sample. The library was prepared using Illumina TruSeq RNA Library Prep Kit v2 (RS-122-2001) according to Manufacturer's protocol. This protocol allows RNA input of 100ng-1000ng. Illumina UMI barcodes were used to multiplex the libraries as per the Manufacturer's instructions. Quality and quantity of each sequencing final library were assessed using Agilent 2100 BioAnalyzer system (Agilent, CA, USA). Total of 10nM picogreen measured library were pooled for 1.3pM loading on the sequencer. The pooled libraries were sequenced on Illumina NexSeq platform in PE75 (75 bp paired end) run with the NextSeq reagent kit v2.5 for 75 cycles. About 30-40 Million sequencing reads were generated per sample for the transcriptome analysis.

Paired end demultiplexed fastq files were generated using bcl2fastq2 (Illumina, v2.17), from NextSeq550 v2.5 reagent's bcl files. Initial quality control was performed using FastQC v0.11.8 and multiqc v1.7. Fastq files were imported batch wise, trimmed for adapter sequences followed by quality trimming using CLC Genomics Workbench (CLC Bio, v23.0.3). The imported high-quality reads were mapped against gene regions and transcripts annotated by ENSEMBL v99 hg38 using the RNA-seq Analysis tool v2.7 (CLC Genomics

Workbench), only matches to the reverse strand of the genes were accepted (using the strand-specific reverse option). Differential gene expression analysis between the sample groups was done using the Differential Expression for RNA-seq tool v2.8, where the normalization method was set as TMM. Differential expression between the groups was tested using a control group, outliers were downweighed, and filter on average expression for FDR correction was enabled.

Gene expression QC, quantification, and DEG analysis. Fastq reads were aligned to the mouse genome (GENCODE Version M27) followed by a multi-step quality control process, which included assessments at the read, mapping, and dataset levels according to RNA sequencing quality control methods previously outlined (53). Gene-level expression quantification utilized HTSeq, and the resulting count data were normalized using voom. Differential gene expression analysis was performed in R using the Limma package (54). The Benjamini & Hochberg method for controlling the false discovery rate was applied as a correction factor for the adjusted p-value. Statistically significant differentially expressed genes (DEGs) were determined based on an adjusted p-value threshold of less than 0.05. All heatmaps were created using the ComplexHeatmap R package (55).

Gene module inference and association with metadata. Independent Component Analysis (ICA) was performed using the Stabilized-ica Python package (version 2.0.0) available at https://github.com/ncaptier/stabilized-ica. This analysis was applied to gene expression data, excluding the TUDCA effect group. Subsequently, the ICA component mixing matrix was correlated with metadata, revealing a significant correlation between IC6 and UCR (p-value < 0.05). The genes contributing to IC6 were identified using an arbitrary threshold value of 3 deviations from the mean of the distribution. A network analysis was then conducted on the resulting set of 253 genes (see Supplemental Figure S2).

Statistical analysis. Student t test and one-way analysis of variance were used to determine statistical significance.

Author contributions

JH and ZL conducted experiments, JH, ZL, OA, and IM acquired data, JH, ZL, MA, CAA, OA, IM, SE, MK, JMH, AN, ANC analyzed data, LAB and PAJ provided critical methods and reagents, AN, ANC and RTM wrote the manuscript, all authors contributed to editing the manuscript.

Acknowledgments

The work published in this manuscript were supported by the National Institutes of Health grant numbers DK083592 (to LAB PAJ, and RTM), and the Charles and Jane Pak Center for Mineral Metabolism and Clinical Research (RTM, ANC).

References

1. Groopman EE, Marasa M, Cameron-Christie S, Petrovski S, Aggarwal VS, Milo-Rasouly H, et al. Diagnostic Utility of Exome Sequencing for Kidney Disease. *N Engl J Med.* 2019;380(2):142-51.

2. Sharif B, and Barua M. Advances in molecular diagnosis and therapeutics in nephrotic syndrome and focal and segmental glomerulosclerosis. *Curr Opin Nephrol Hypertens.* 2018;27(3):194-200.

3. Papazachariou L, Demosthenous P, Pieri M, Papagregoriou G, Stavrou C, Zavros M, et al. Frequency of COL4A3/COL4A4 mutations amongst families segregating glomerular microscopic hematuria and evidence for activation of the unfolded protein response. Focal and segmental glomerulosclerosis is a frequent development during aging. *PLoS ONE.* 2014;9(12):e115015.

4. Deltas C, Savva I, Voskarides K, Papazachariou L, and Pierides A. Carriers of Autosomal Recessive Alport Syndrome with Thin Basement Membrane Nephropathy Presenting as Focal Segmental Glomerulosclerosis in Later Life. *Nephron.* 2015;130(4):271-80.

5. Greka A, and Mundel P. Cell Biology and pathology of podocytes. *AnnRevPhysiol.* 2012;74:299-323.

6. Hu M, Azeloglu EU, Ron A, Tran-Ba KH, Calizo RC, Tavassoly I, et al. A biomimetic gelatin-based platform elicits a pro-differentiation effect on podocytes through mechanotransduction. *Scientific reports.* 2017;7:43934.

7. Rogg M, Maier JI, Van Wymersch C, Helmstädter M, Sammarco A, Lindenmeyer M, et al. α-Parvin Defines a Specific Integrin Adhesome to Maintain the Glomerular Filtration Barrier. *J Am Soc Nephrol.* 2022.

8. Maier JI, Rogg M, Helmstädter M, Sammarco A, Schilling O, Sabass B, et al. EPB41L5 controls podocyte extracellular matrix assembly by adhesome-dependent force transmission. *Cell Rep.* 2021;34(12):108883.

9. Schell C, and Huber TB. The Evolving Complexity of the Podocyte Cytoskeleton. *J Am Soc Nephrol.* 2017;28(11):3166-74.

10. Embry AE, Liu Z, Henderson JM, Byfield FJ, Liu L, Yoon J, et al. Similar Biophysical Abnormalities in Glomeruli and Podocytes from Two Distinct Models. *J Am Soc Nephrol.* 2018;29(5):1501-12.

11. Embry AE, Mohammadi H, Niu X, Liu L, Moe B, Miller-Little WA, et al. Biochemical and Cellular Determinants of Renal Glomerular Elasticity. *PLoS One.* 2016;11(12):e0167924.

12. Rinschen MM, Grahammer F, Hoppe AK, Kohli P, Hagman H, Kretz O, et al. YAP-mediated mechanotransduction determines the podocyte's response to damage. *Sci Signaling.* 2017;10:eaaf8165.

13. Wyss HM, Henderson JM, Byfield FJ, Bruggeman LA, Ding Y, Huang C, et al. Biophysical properties of normal and diseased renal glomeruli. *AmJPhysiol(Cell).* 2011;300:C397-C405.

14. Azeloglu EU, Hardy SV, Eungdamrong NJ, Chen Y, Jayaraman G, Chuang PY, et al. Interconnected network motifs control podocyte morphology and kidney function. *Science signaling.* 2014;7(311):ra12.

15. Calizo RC, Bhattacharya S, van Hasselt JGC, Wei C, Wong JS, Wiener RJ, et al. Disruption of podocyte cytoskeletal biomechanics by dasatinib leads to nephrotoxicity. *Nature communications.* 2019;10(1):2061.

16. Gyarmati G, Shroff UN, Izuhara A, Hou X, Da Sacco S, Sedrakyan S, et al. Intravital imaging reveals glomerular capillary distension and endothelial and immune cell activation early in Alport syndrome. *JCI Insight.* 2022;7(1).

17. Ding F, Wickman L, Wang SQ, Zhang Y, Wang F, Afshinnia F, et al. Accelerated podocyte detachment and progressive podocyte loss from glomeruli with age in Alport Syndrome. *Kidney Int.* 2017;92(6):1515-25.

18. Kriz W, Hähnel B, Hosser H, Rösener S, and Waldherr R. Structural analysis of how podocytes detach from the glomerular basement membrane under hypertrophic stress. *Front Endocrinol (Lausanne).* 2014;5:207.

19. Cosgrove D, Kalluri R, Miner JH, Segal Y, and Borza DB. Chosing a mouse model to study the molecular pathobiology of Alport glomerulonephritis. *Kidney International.* 2007;71:615-8.

20. Andrews KL, Mudd JL, Li C, and Miner JH. Quantitative trait loci influence renal disease progression in a mouse model of Alport syndrome. *AmJPath.* 2002;160(2):721-30.

21. Miner JH, and Sanes JR. Molecular and functional defects in kidneys from mice lacking collagen ‡3(IV): implications for Alport syndrome. *JCell Biol.* 1996;135(5):1403-13.

22. Schell C, Rogg M, Suhm M, Helmstädter M, Sellung D, Yasuda-Yamahara M, et al. The FERM protein EPB41L5 regulates actomyosin contractility and focal adhesion formation to maintain the kidney filtration barrier. *Proc Natl Acad Sci U S A.* 2017;114(23):E4621-e30.

23. Pieri M, Stefanou C, Zavarinos A, Erguler K, Stylianou K, Lapathitis G, et al. Evidence for activation of the unfolded protein resppnse in collagen IV nephropathies. *JASN.* 2014;25:260-75.

24. Kusaczuk M. Tauroursodeoxycholate-Bile Acid with Chaperoning Activity: Molecular and Cellular Effects and Therapeutic Perspectives. *Cells.* 2019;8(12).

25. Rani S, Sreenivasaiah PK, Kim JO, Lee MY, Kang WS, Kim YS, et al. Tauroursodeoxycholic acid (TUDCA) attenuates pressure overload-induced cardiac remodeling by reducing endoplasmic reticulum stress. *PLoS One.* 2017;12(4):e0176071.

26. Panda DK, Bai X, Zhang Y, Stylianesis NA, Koromilas AE, Lipman ML, et al. SCF-SKP2 E3 ubiquitin ligase links mTORC1/ER stress/ISR with YAP activation in murine renal cystogenesis. *J Clin Invest.* 2022;132(24).

27. Levental I, Levental KR, Klein EA, Assoian R, Miller RT, Wells RG, et al. A simple indentation device for measuring micrometer-scale tissue stiffness. *Journal of Physics: Condensed Matter.* 2010;22:191420.

28. Ge X, Zhang T, Yu X, Muwonge AN, Anandakrishnan N, Wong NJ, et al. LIM-Nebulette Reinforces Podocyte Structural Integrity by Linking Actin and Vimentin Filaments. *J Am Soc Nephrol.* 2020.

29. Liu Z, Yoon J, Wichaidit C, Jaykumar AB, Dbouk HA, Embry AE, et al. Control of Podocyte and Glomerular Capillary Wall Structure and Elasticity by WNK1 Kinase. *Front Cell Dev Biol.* 2020;8:618898.

30. Evangelista JE, Xie Z, Marino GB, Nguyen N, Clarke DJB, and Ma'ayan A. Enrichr-KG: bridging enrichment analysis across multiple libraries. *Nucleic Acids Res.* 2023;51(W1):W168-W79.

31. Li X, Bechara R, Zhao J, McGeachy MJ, and Gaffen SL. IL-17 receptor-based signaling and implications for disease. *Nat Immunol.* 2019;20(12):1594-602.

32. Krebs CF, Reimers D, Zhao Y, Paust HJ, Bartsch P, Nuñez S, et al. Pathogen-induced tissue-resident memory T(H)17 (T(RM)17) cells amplify autoimmune kidney disease. *Sci Immunol.* 2020;5(50).

33. Allen JE. IL-4 and IL-13: Regulators and Effectors of Wound Repair. *Annu Rev Immunol.* 2023;41:229-54.

34. Kim AH, Chung JJ, Akilesh S, Koziell A, Jain S, Hodgin JB, et al. B cell-derived IL-4 acts on podocytes to induce proteinuria and foot process effacement. *JCI Insight.* 2017;2(21).

35. Lai KW, Wei CL, Tan LK, Tan PH, Chiang GS, Lee CG, et al. Overexpression of interleukin-13 induces minimal-change-like nephropathy in rats. *J Am Soc Nephrol.* 2007;18(5):1476-85.

36. Abrahamson DR, Hudson BG, Stroganova L, Borza DB, and St John PL. Cellular origins of type IV collagen networks in developing glomeruli. *J Am Soc Nephrol.* 2009;20(7):1471-9.

37. Wiseman RL, Mesgarzadeh JS, and Hendershot LM. Reshaping endoplasmic reticulum quality control through the unfolded protein response. *Mol Cell.* 2022;82(8):1477-91.

38. Marutani T, Yamamoto A, Nagai N, Kubota H, and Nagata K. Accumulation of type IV collagen in dilated ER leads to apoptosis in Hsp47-knockout mouse embryos via induction of CHOP. *J Cell Sci.* 2004;117(Pt 24):5913-22.

39. Uppala JK, Gani AR, and Ramaiah KVA. Chemical chaperone, TUDCA unlike PBA, mitigates protein aggregation efficiently and resists ER and non-ER stress induced HepG2 cell death. *Scientific reports.* 2017;7(1):3831.

40. Wang D, Mohammad M, Wang Y, Tan R, Murray LS, Ricardo S, et al. The Chemical Chaperone, PBA, Reduces ER Stress and Autophagy and Increases Collagen IV α5 Expression in Cultured Fibroblasts From Men With X-Linked Alport Syndrome and Missense Mutations. *Kidney Int Rep.* 2017;2(4):739-48.

41. Lo AC, Callaerts-Vegh Z, Nunes AF, Rodrigues CMP, and D'Hooge R. Tauroursodeoxycholic acid (TUDCA) supplementation prevents cognitive impairment and amyloid deposition in APP/PS1 mice. *Neurobiology of Disease.* 2013;50:21-9.

42. Jarad G, Knutsen RH, Mecham RP, and Miner JH. Albumin contributes to kidney disease progression in Alport syndrome. *Am J Physiol Renal Physiol.* 2016;311(1):F120-30.

43. Venkatareddy M, Wang S, Yang Y, Patel S, Wickman L, Nishizono R, et al. Estimating podocyte number and density using a single histologic section. *J Am Soc Nephrol.* 2014;25(5):1118-29.

44. Cervenka L, Mitchell KD, and Navar LG. Renal function in mice: effects of volume expansion and angiotensin II. *J Am Soc Nephrol.* 1999;10(12):2631-6.

45. Cortes P, Zhao X, Riser BL, and Narins RG. Regulation of glomerular volume in normal and partially nephrectomized rats. *AmJPhysiol(Renal Physiol).* 1996;270:F356-F70.

46. Kashtan CE, and Gross O. Clinical practice recommendations for the diagnosis and management of Alport syndrome in children, adolescents, and young adults-an update for 2020. *Pediatr Nephrol.* 2021;36(3):711-9.

47. Wiggins JE, Goyal M, Sanden SK, Wharram BL, Shedden KA, Misek DE, et al. Podocyte hypertrophy, "adaptation," and "decompensation" associated with glomerular enlargement and glomerulosclerosis in the aging rat: prevention by calorie restriction. *J Am Soc Nephrol.* 2005;16(10):2953-66.

48. Aypek H, Krisp C, Lu S, Liu S, Kylies D, Kretz O, et al. Loss of the collagen IV modifier prolyl 3-hydroxylase 2 causes thin basement membrane nephropathy. *J Clin Invest.* 2022;132(9).

49. Wiggins JE, Goyal M, Sanden SK, Wharram BL, Shedden KA, Misek DE, et al. Podocyte hypertrophy, "adaptation," and "decompensation" associated with glomerular enlargement and glomerulosclerosis in the aging rat: prevention with caloric restrictuion. *JASN.* 2005;16:2953-66.

50. Schlondorff D. Preparation and study of isolated glomeruli. *Methods in Enzymology.* 1990;191:130-40.

51. Naldini L, Blömer U, Gallay P, Ory D, Mulligan R, Gage FH, et al. In vivo gene delivery and stable transduction of nondividing cells by a lentiviral vector. *Science.* 1996;272(5259):263-7.

52. Shankland SJ, Pippin JW, Reiser J, and Mundel P. Podocytes in culture: past, present, and future. *Kidney Int.* 2007;72(1):26-36.

53. Hong C, Eichinger F, Atta MG, Estrella MM, Fine DM, Ross MJ, et al. Viral associations with kidney disease diagnosis and altered kidney metatranscriptome by kidney function. *Kidney Int.* 2023;103(1):218-22.

54. Ritchie ME, Phipson B, Wu D, Hu Y, Law CW, Shi W, et al. limma powers differential expression analyses for RNA-sequencing and microarray studies. *Nucleic Acids Res.* 2015;43(7):e47.

55. Gu Z. Complex heatmap visualization. *iMeta.* 2022;1(3):e43.

Figures

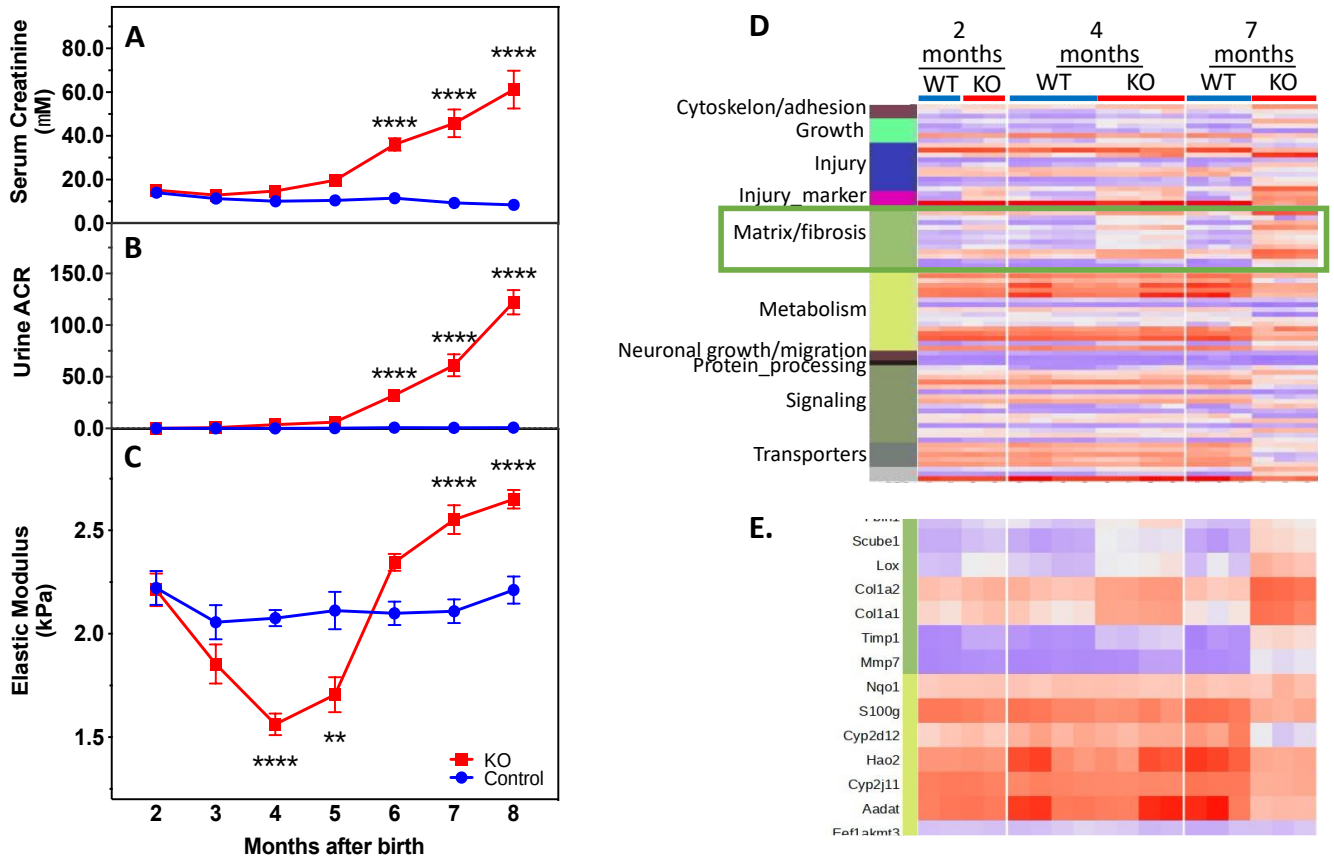

Figure 1. Measurement of serum creatinine (**A**), urine ACR (**B**), and glomerular elastic modulus (E, Young's modulus) (**C**) in Col4α3$^{-/-}$ (KO, red) mice over the course of renal disease compared to wildtype or heterozygote controls (Control, blue). Beginning two months after birth, serum creatine (µM) and urine ACR (mg/g) were measured monthly through eight months. Glomerular E (kPa) was measured in mice sacrificed at indicated time point using micro indentation of isolated glomeruli. Each point in graphs show average E values from 4 - 12 different mice. Average glomerular E for each mouse was calculated from 6-10 glomeruli. Significance was determined by 2-way ANOVA using Graphpad; **P<0.01, ****P<0.0001. **(D)** Differentially expressed genes in KO kidneys at 2, 4, and 7 months compared to age-matched Control. N=2 per group at 2 months, 4 per group at 4 months, and 3 per group at 7 months. **(E)** – has some collagen/fibrosis genes, but most are not.

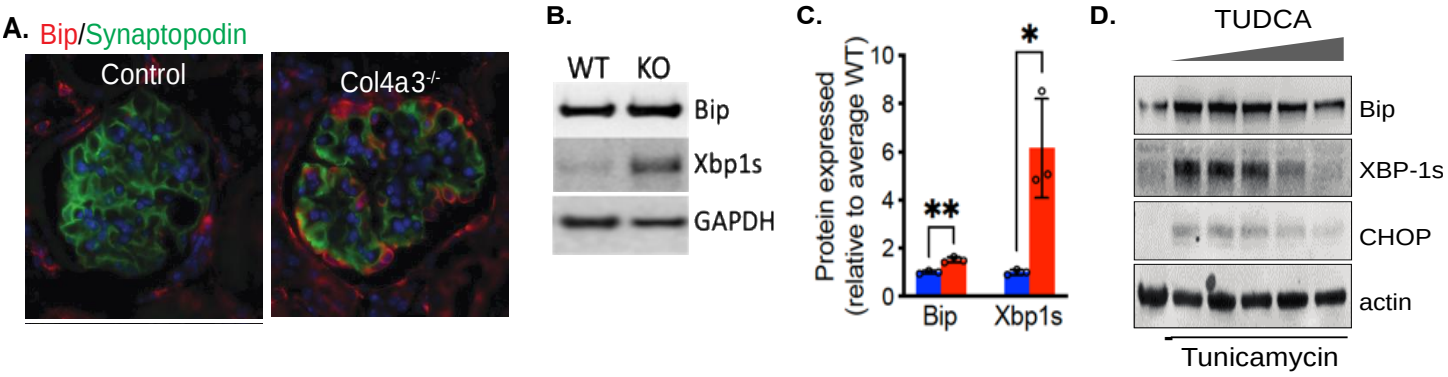

Figure 2. Evidence of UPR activation in glomeruli and podocytes from Col4α3$^{-/-}$ mice. A) IF images of Bip and synaptopodin staining in 4 month Control and Col4α3$^{-/-}$ mouse glomeruli, B) Blots of UPR markers in podocyte cell lines under basal conditions derived from WT and Col4α3$^{-/-}$ (KO) mice. The cells were maintained under standard conditions, harvested in RIPA buffer at 7% confluence, and the crude extract was immunoblotted with antibodies against bip, Xbp1s, and GAPDH. C) Comparison of Bip and Xbp1s protein expression from B (N=3, normalized to WT). D) Efficacy of TUDCA for blocking tunicamycin-induced of UPR marker expression in WT podocytes. Podocytes were treated with tunicamycin 1 μg/ml and then increasing concentrations of TUDCA from 1 - 4 mM for four hours.

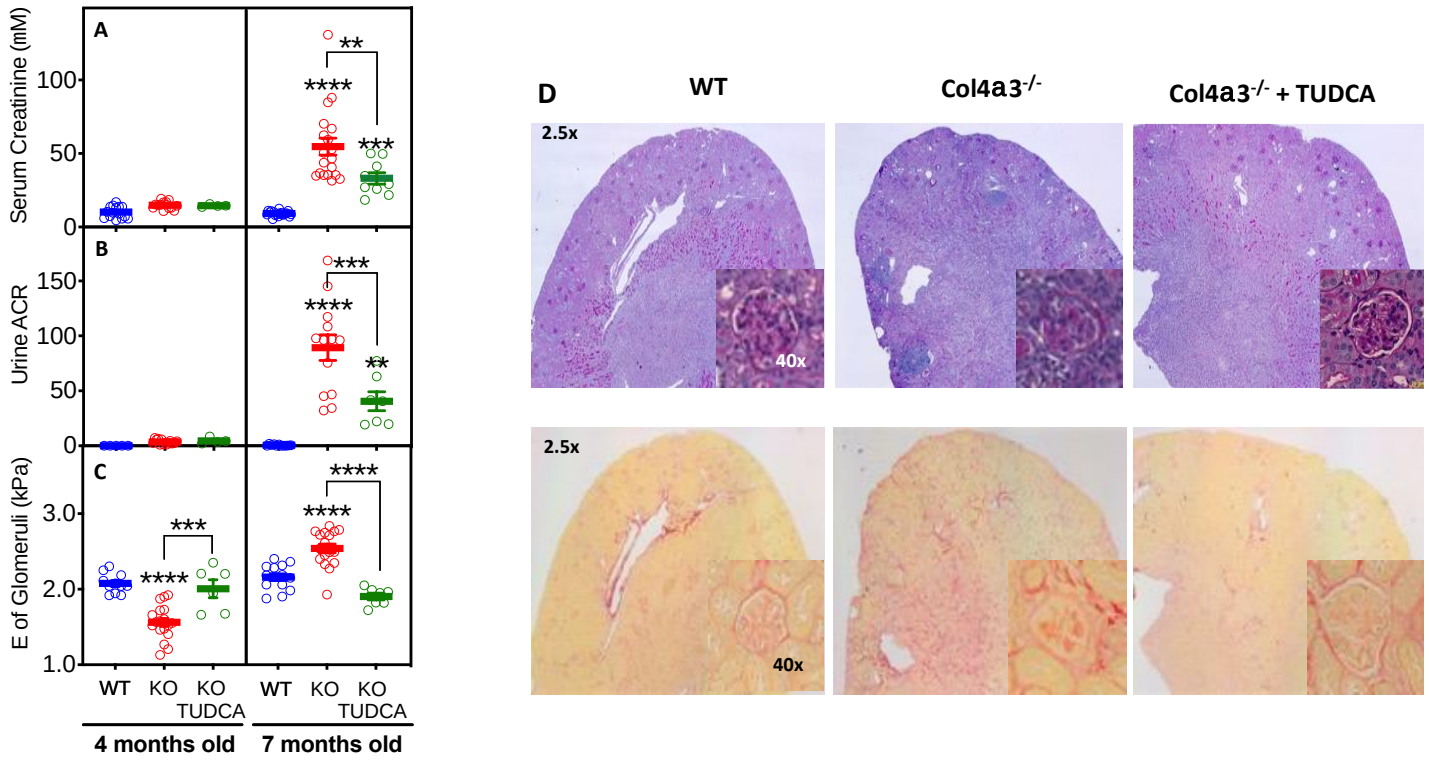

Figure 3. TUDCA treatment slows progression of renal disease and attenuates the decrease in E in Col4α3$^{-/-}$ mice. KO mice were treated from weaning (approximately 4 weeks), with 0.8% TUDCA mouse chow. **2A.** At 4 and 7 months of age, serum creatine (µM), urine ACR, and glomerular elastic modulus (E, kPa) was measured in Control, KO and TUDCA treated KO animals. Each circle represents the average of 6-10 independent E of glomeruli from a distinct mouse. Significance was determined by ANOVA and multiple comparisons test using GraphPad; **P<0.01,***P<0.001, ****P<0.0001. **2B.** Comparison of kidney cortex from Control, KO, and TUDCA treated KO animals. A) Histopathology of mouse kidney sections at 7 months of age as indicated.

A.

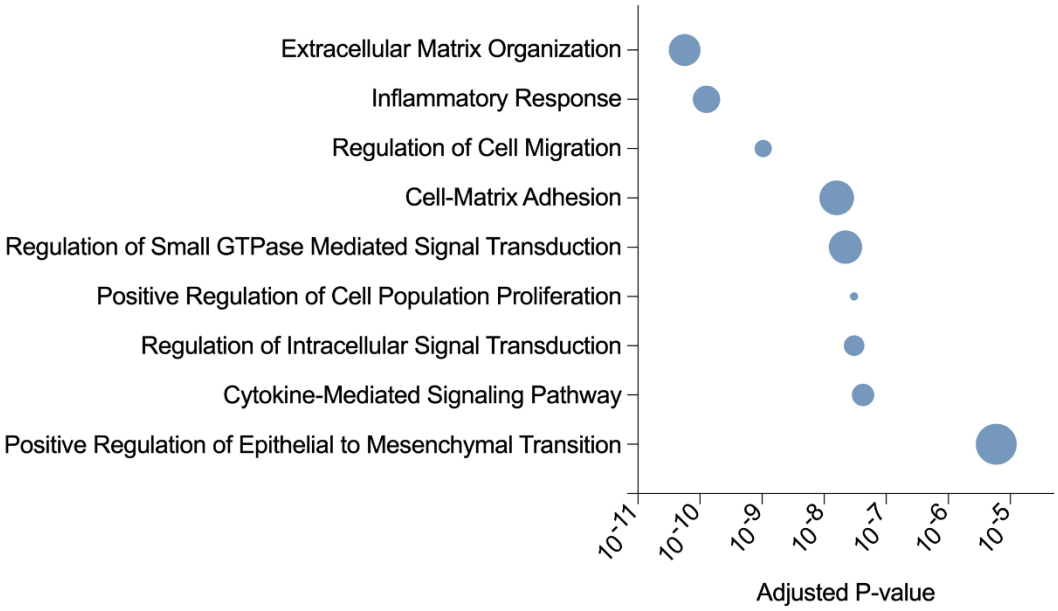

B.

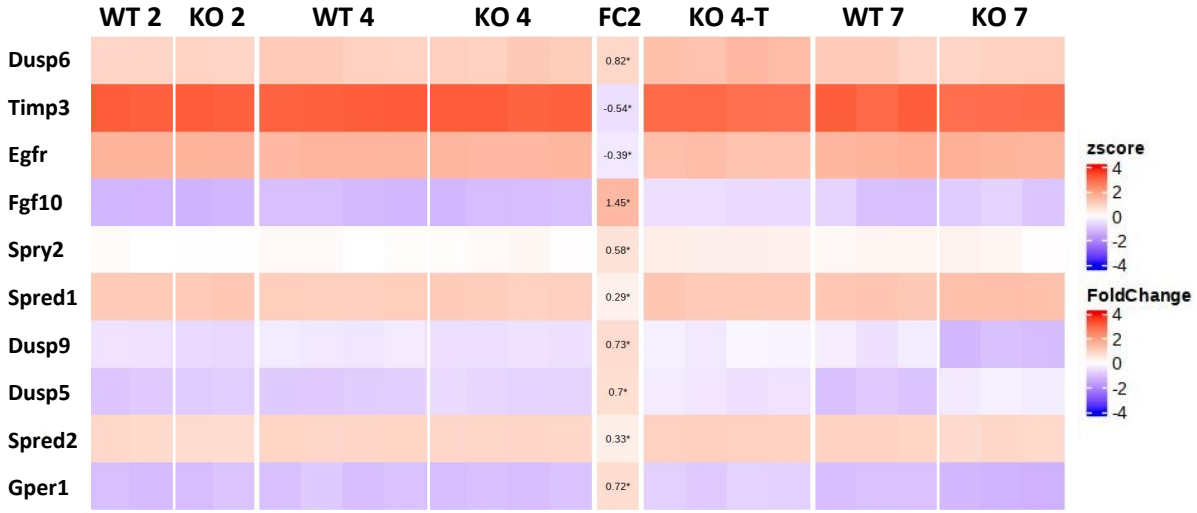

Figure 4. A) Summary of Gene Ontology categories that are over-represented by DEGs from 4 month old WT and KO PE-75 RNAseq comparison assembled by ENRICHR. B) Heatmap of genes related to ERK signaling pathway identified from KO and KO-T DEGs. The heatmap shows the samples across the top, WT and Col4α3$^{-/-}$ (KO) at 2 months (2 samples each), WT and KO 4 months (four samples each) and Col4α3$^{-/-}$ + TUDCA (KO-T) 4 months with four samples, and WT and KO at 7 months each with three samples. The column under FC shows the direction and magnitude of expression change from KO to KO-T, and * denotes significance <0.05 (Complex Heatmap R Package).

Gene	Control (N)	KO (N)	KO_TUDCA (N)
Col1α1	1 (3)	55.5 +/- 13 (5)	26.2 +/- 6.2 (4)
Col1α2	1 (5)	29.6 +/- 7.3 (5)	13.9 +/- 3.2 (4)
Col3α1	1 (3)	74.1 +/- 15 (5)	31.9 +/- 2.4 (4)
LOX	1 (4)	29.7 +/- 7.4 (3)	13.3 +/- 7.6 (4)
LOXL2	1 (4)	21.5 +/- 7.1 (3)	6.7 +/- 3.1 (4)
TNFα	1 (4)	30.3 +/- 7.9 (3)	14.3 +/- 3.0 (4)
TGF-β1	1 (3)	4.80 +/- 0.8 (4)	3.0 +/- 0.7 (4)
EGF	1 (3)	0.20 +/- 0.1 (5)	0.7 +/- 0.2 (4)
Cyr61	1 (5)	4.46 +/- 0.6 (3)	2.0 +/- 1.0 (4)

Table 1. Summary of qRT-PCR of selected fibrosis or injury-related genes in 7 months old KO mice with and without TUDCA treatment compared to age-matched WT littermates. All values in KO and KO-TUDCA groups represent fold change from WT control and were significantly different from Control, as determined by ANOVA.

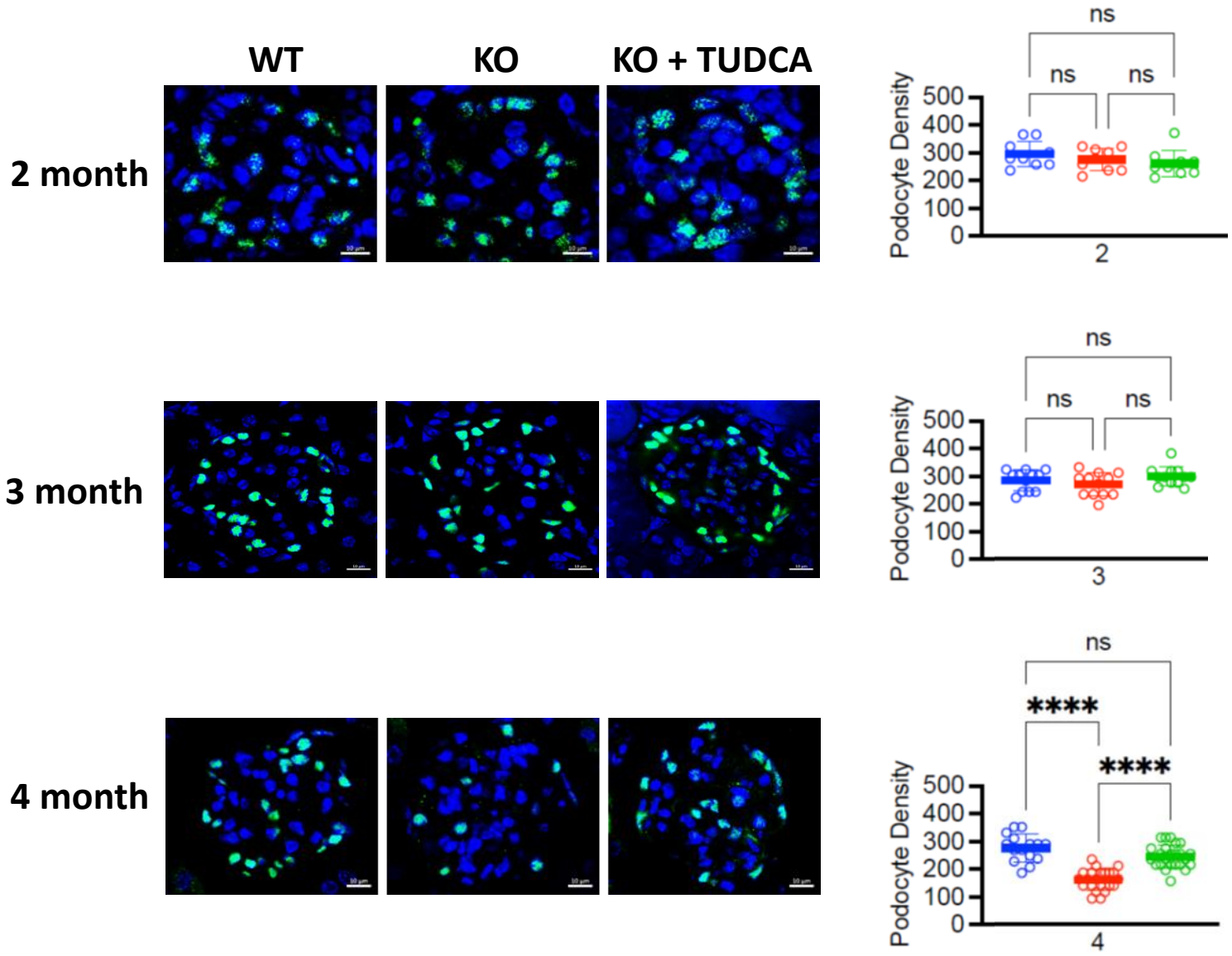

Figure 5. TUDCA reduces podocyte loss from Col4α3$^{-/-}$ mouse glomeruli. A) Representative glomeruli in kidney sections from Control, Col4α3$^{-/-}$, and TUDCA-treated Col4α3$^{-/-}$ mice from 2, 3, and 4 months old mice were stained for WT-1 and DAPI. Scale bar: 10 μm. **B)** Summary of podocyte density analysis. The number of WT-1 and DAPI-positive nuclei in 20 glomeruli from 3 mice were counted and used for podocyte density calculations. Each dot represents the number of WT-1 positive nuclei in a single glomerulus. Data are shown as mean ± SEM and significance was determined by ordinary one-way ANOVA, followed by Dunnett's multiple comparisons test; ****P<0.0001.

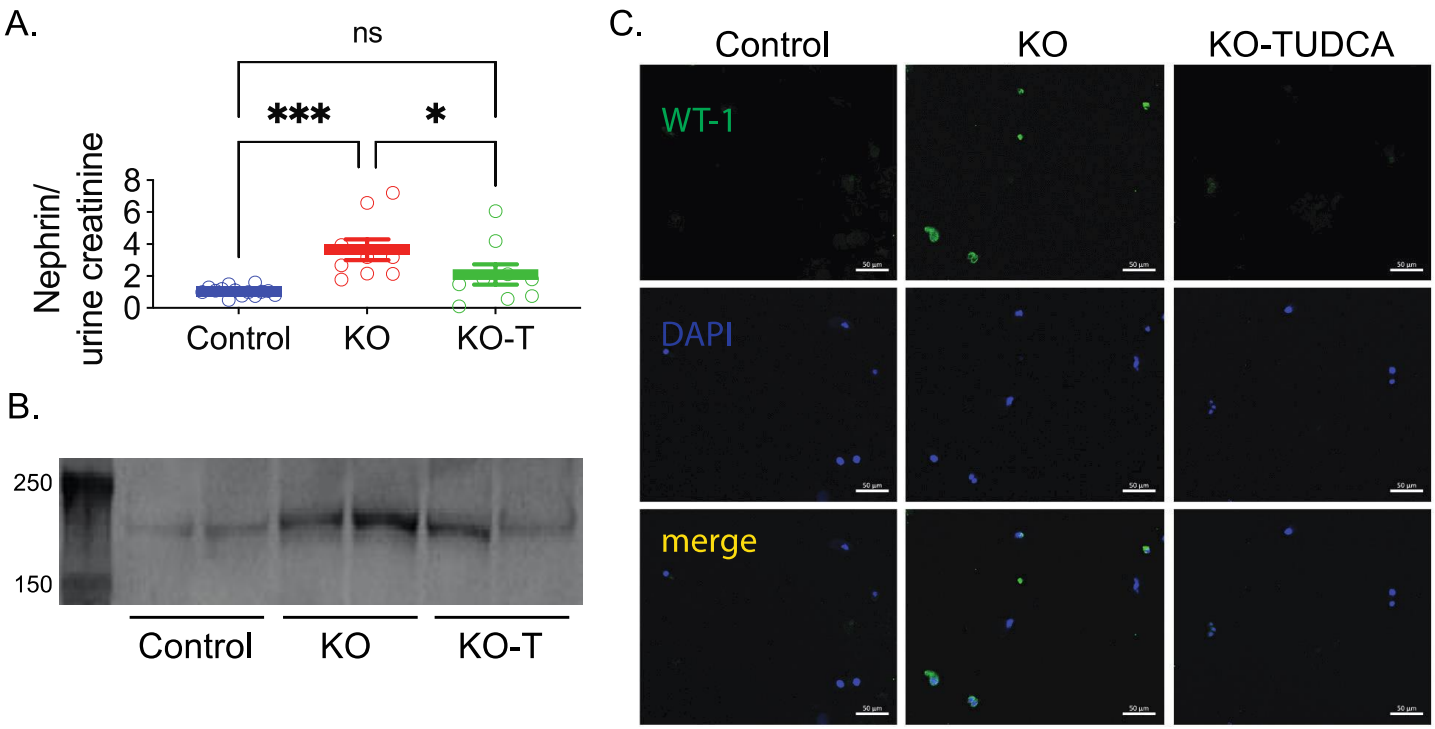

Figure 6. Glomerular capillary deformability and podocytes adhesion. Control, KO, and TUDCA-treated KO mice were injected (IP) with approximately 1 ml of saline, and urine was collected over the subsequent two hours. The urine samples were normalized for creatinine, immunoblotted for nephrin, and quantitated with densitometry. The pellet was stained for WT-1 and DAPI. A) shows aggregate data for all samples groups expressed as nephrin/creatinine (arbitrary densitometry units for nephrin) for each sample group. Each point represents a sample from a single mouse, bar indicates mean ± SEM. Significance was determined by ordinary one-way ANOVA, followed by Tukey's multiple comparisons test; *P<0.05, ***P<0.001. B) Summary data for urine nephrin immunoblot C. Representative nephrin immunoblot showing duplicate samples from each group, and C. showing representative urine sediment samples stained for WT-1 and DAPI.

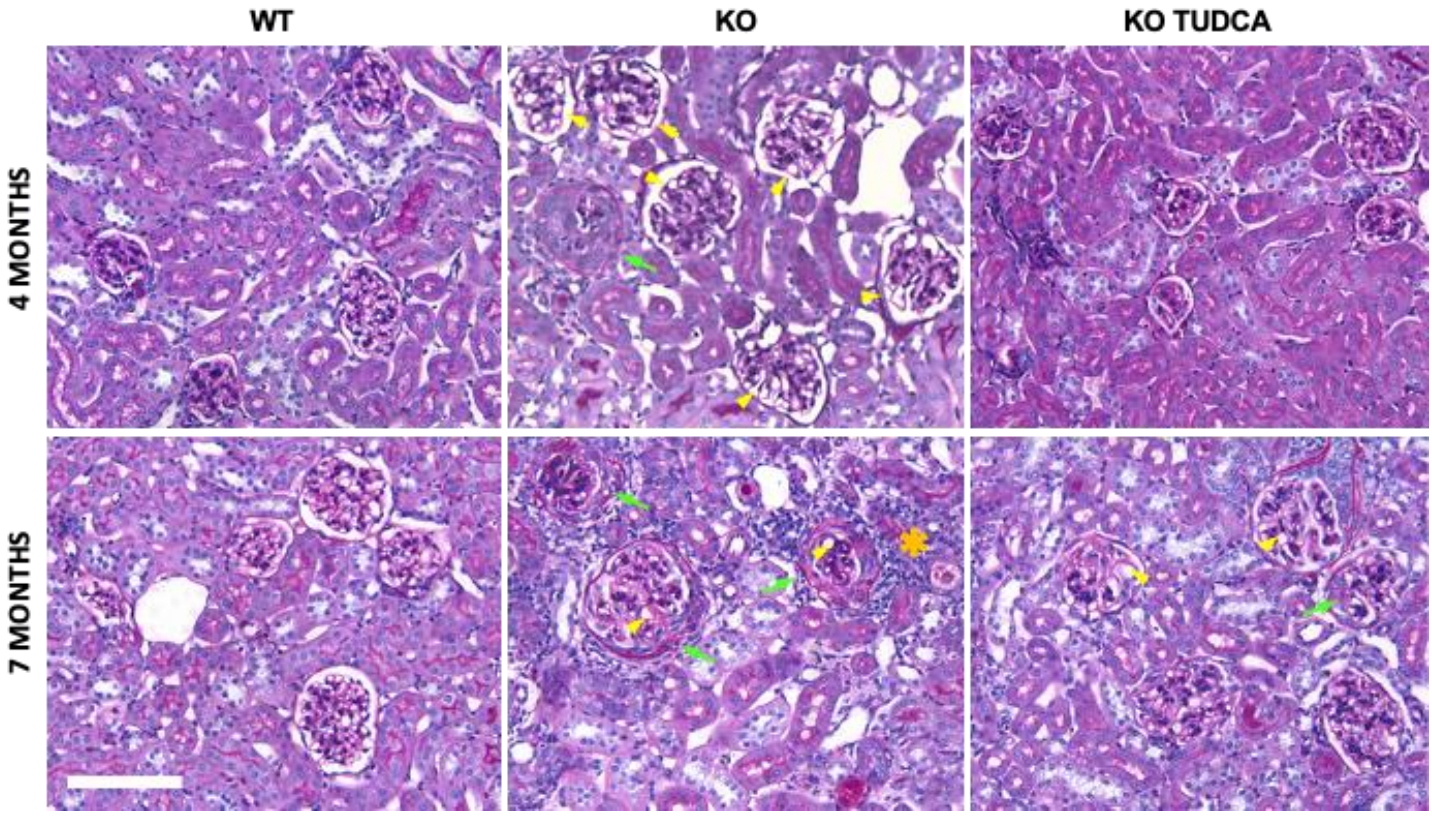

Figure 7. Brightfield photomicrographs of PAS-stained kidney sections kidneys from 4 months (top row) and 7 months old Control mice, Col4α3$^{-/-}$ (KO), and TUDCA-treated Col4α3$^{-/-}$ (KO TUDCA) mice. The 4 month KO image shows glomerular enlargement and focal proliferative glomerular lesions (green arrow), and distension of glomerular capillary lumens (yellow arrowheads) that are not observed in Control (top left) or the TUDCA treated KO mice (top right). The 7 month KO mice (bottom center) show more extensive glomerular proliferative lesion development (green arrows), with proliferation composed predominantly of epithelial cells filling Bowman's space, along with patchy areas of tubular atrophy and interstitial fibrosis and chronic inflammation (orange asterisk). The section from the 7 month TUDCA-treated mice show evidence of glomerular injury with PAS stain; bar = 200 µm for all images.

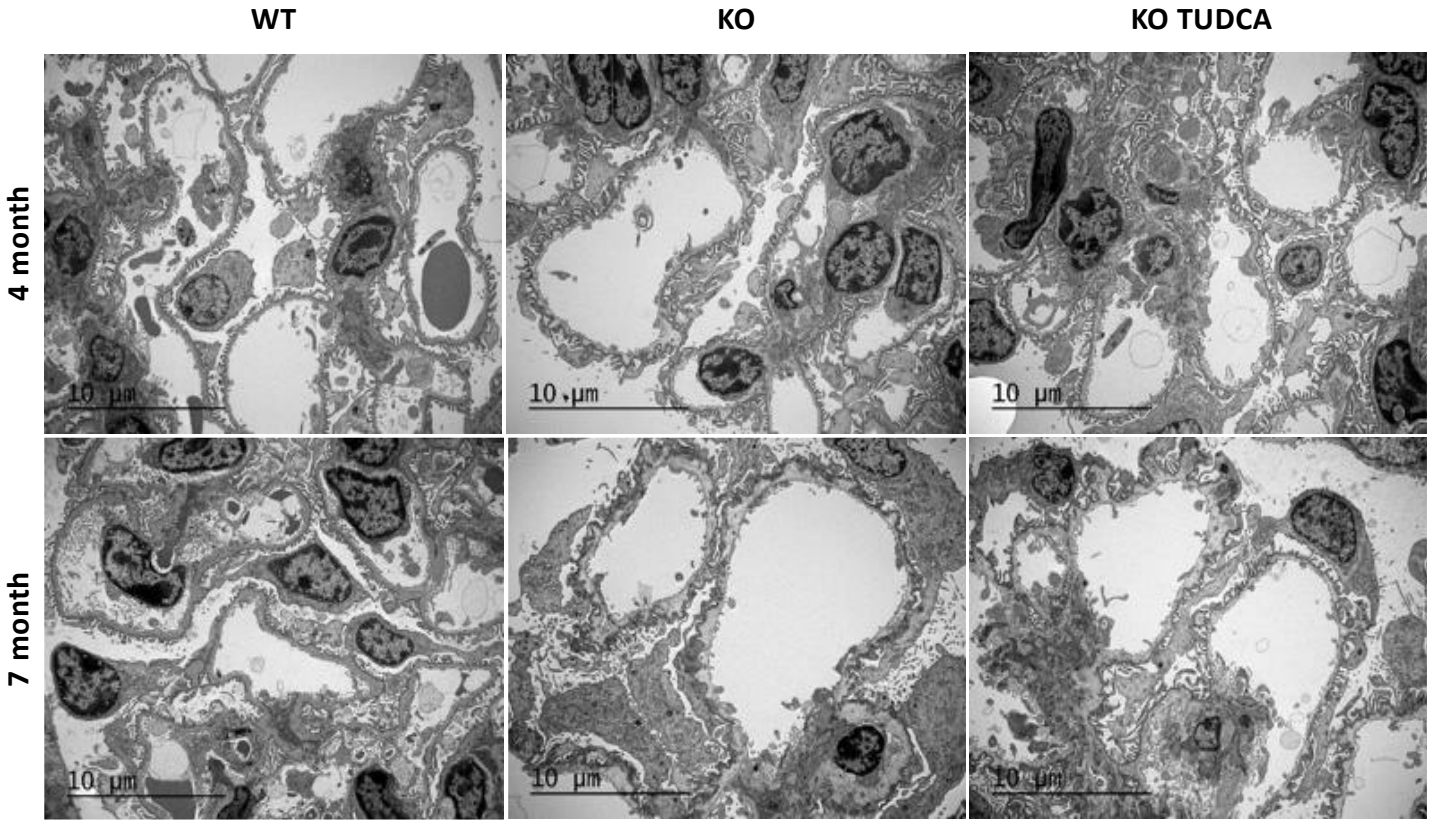

Figure 8. Transmission Electron micrographs of mouse kidneys, showing glomerular changes at 4 (top row) and 7 (bottom row) months in Control, Col4α3$^{-/-}$ (KO), and TUDCA-treated Col4α3$^{-/-}$ (KO TUDCA) mice. At 4 months, glomeruli of KO mice (top center) and KO TUDCA mice (top right) reveal features of segmental podocyte injury, including mild segmental podocyte foot process effacement, more extensive but segmental foot process irregularity, and mild microvillous change. These podocyte changes are concurrent with segmentally prominent "knob-like" subepithelial basement redundancy, characteristic of the Col4α3 -/- mouse model. Control mice (top left) show none of these changes. At 7 months (bottom row), KO mice (bottom center) reveal more severe and widespread podocyte injury, demonstrated by extensive podocyte foot process effacement and irregularity, cellular hypertrophy, and microvillous change. There are also comparable glomerular basement membrane changes including extensive subepithelial basement redundancy and segmental "basket weaving", and segmental glomerular capillary loop dilation. In contrast, KO TUDCA mice (bottom right) show podocyte and glomerular basement membrane changes that are similar in nature to those of the KO mice but are less extensive and more segmental. None of these changes are seen in Control mice (bottom left). All images are the same magnification – scale bar = 10 µm.